2014 International Conference on Unmanned Aircraft Systems (ICUAS)
May 27-30, 2014. Orlando, FL, USA

Optimal Collection of High Resolution Aerial Imagery with Unmanned Aerial Systems

Brandon Stark, *Student Member, IEEE*, YangQuan Chen, *Senior Member, IEEE*

***Abstract*—Remote sensing applications are an emerging topic for Unmanned Aerial Systems (UASs). Unlike many remote sensing image collection methods, UASs have several advantages when it comes to on demand data acquisition. Relatively low operating costs, high portability and low flight altitudes make UASs excellent tools for researchers to collect high resolution imagery where satellites or manned aircraft are inefficient. In particular areas, such as in rangelands, the use of UASs to aid in management practices could have significant benefit. However, in these areas, current methodologies of remote sensing utilizing spectral reflectance data for vegetation analysis have performed poorly due to the high spatial and low spectral heterogeneity of the area. One of the root causes of the poor performance can be traced to the negative effect of shadows that are interspersed in the spectral reflectance data. The unique advantage of low infrastructure and minimal downtime for UASs enables researchers to exert greater control over the precise time of data collection. In this paper, it is demonstrated that the time of imagery collection can be optimized with regards to the minimization of shadows found in the imagery. The process described in this paper utilizes a high resolution digital elevation map (DEM) that can be generated through photogrammetry techniques to create an estimate of shadows given a time of day at a known location. Furthermore, the results of estimated shadow map can be utilized for improving classification techniques without additional equipment.**

***Index Terms*—Unmanned Aerial System, remote sensing, rangeland management, natural resource management, imagery optimization**

I. Introduction

THE land classified as rangelands comprise of over half of the usable land in the world and have significant agricultural and economic value. Conservation and management of these lands can be a challenging task due to the wide variety of activity and large areas [1]. Satellite imagery can be used for decision support, but the resolution of the imagery is typically insufficient. Finer details such as individual vegetation and small water features are impossible to see and become difficult for management. Accurate assessment of small features, such as dead matter or litter have been identified as one of the most important indicators for assessing long-term sustainability of the land [2]. Current methods, using satellites or field-crews, suffer from high costs and limited actionable intelligence due to the sparse nature of the evaluations.

School of Engineering, University of California, Merced, Merced, CA, USA, e-mail: bstark2@ucmerced.edu
School of Engineering, University of California, Merced, Merced, CA, USA, e-mail: ychen53@ucmerced.edu

Unmanned Aerial Systems (UASs) provide a new and cost efficient method for data collection for better rangeland management [2–4]. These autonomous systems have several advantages over satellite imagery or manned aircraft. They can fly at very low altitudes, enabling high resolution imagery, can accomplish a wide variety of mission and can be much safer and cheaper to operate. As a result, remote sensing applications for UASs have seen significant growth as their utility gains credibility.

One of the lesser discussed advantages of UASs is that due to the low infrastructure requirements and minimal downtime of many small UASs, these highly portable systems enables researchers to exert a greater level of control over when imaging data can be collected. If the time at which imagery data is collected can be controlled, then there is some methodology that can be applied to find the optimal time for imagery collection. While much can be discusses in terms of optimizing for peak response, flight altitude or image overlap [5–7], additional optimization can be applied to the minimization of shadows present in the imagery. Shading effects have known negative effects on vegetation and soil metrics and subsequent calculations and classifications that are necessary for analysis [8–10]. In areas with sparse, non-uniform vegetation, the minimization of shadows in imagery is especially valuable.

The minimization of shadows in imagery is intended to improve the performance of many remote sensing classification techniques. While in other ecosystems, automated pixel-based classification techniques based on spectral reflectance have been successfully used [9,11], the same techniques have struggled to perform similarly to traditional methods in rangelands [2]. Traditional line-point intercept (LPI), which involves counting the number of occurrences of the target in a line in the area and extrapolating for the entire area, has maintained a significant advantage in both simplicity and accuracy over most other techniques [2]. It has only been recently with the utilization of object-based classification techniques that automated methods have seen a comparable performance to LPI [4].

Compared to more common UAS remote sensing applications, rangelands pose a significantly more challenging classification operation. Within a rangeland environment, the vegetation is typically sparse and with a high level of heterogeneity. The soil and bareground, likewise, is often a varied mix of clays, rocks and dirt. With pixel based classification strategies, often the difference between two

978-1-4799-2376-2/14/$31.00 ©2014 IEEE

adjacent parts of a shrub is equal to the difference between the shrub and a rock. This lack of separability results in poor classification performance, especially with the use of high resolution imagery that a UAS is capable of providing. A similar problem of separability was apparent in the classification of land cover for forest fire management mapping of potential fuel types [12]. Utilizing LiDAR data in the form of vertical density distributions including the canopy height model with surface reflectance data increased the performance of their classification techniques. Unfortunately, for many UASs, a LiDAR unity is both too costly and too large to implement as a payload simultaneously with imaging equipment.

However, a similar data set can be derived through existing photogrammetry techniques. Photogrammetry, or the science of analyzing images, is a well-established field from which existing techniques can be leveraged for new applications enabled by UASs. The mosaicing of images to create a geo-rectified orthophoto for remote sensing applications is one of the major photogrammetry techniques already in use by UAS operators. As UAS operations have matured, operators have begun leveraging a second major form of photogrammetry technique of utilizing sufficiently overlapping images to generate a digital elevation model (DEM) [10]. The generation of a DEM can be done either through simultaneous imaging from a stereo pair of cameras or through Structure-from-Motion (SfM) algorithms from a single camera. In either method, image points are matched from each pair of images to generate a mapping of pixel distances from the camera. With proper ground control points (GCPs) and georectification, a georectified DEM can be generated [10,13,14].

Recent research has validated the use of UASs for DEM generation by demonstrating an adequate level of accuracy [13,14]. In [14], researchers utilized a commercially available software package, Agisoft Photoscan, to achieve a respectable level of accuracy compared to ground truth measurements with improvement possible with additional processing and GCPs. Another study indicated that the greatest factor in the accuracy of a DEM generated by a UAS was the flight altitude [13]. Other studies have shown similar results using UASs for DEM generation for mapping ice flows [15] and post damage analysis [16]. One significant advantage of the process of generating a DEM is that it can be accomplished through the same set of imagery utilized for spectral reflectance indices or classification, maximizing the use of a single set of imagery collected from a UAS operation. The DEM generation and the shadow estimation described in this paper is realizable without the need to add additional equipment or sensors.

In this paper, the use of a DEM is shown to provide additional data to the object-based classifier in the form of a shadow estimator and enables the collection of imagery at the optimal time. In the event that the time of the imagery is unknown, it is shown that a global search algorithm can be implemented to find the correct sun azimuth and elevation by a comparison with imagery from the near-infrared (NIR) band. The accuracy of the sun position estimation validates the use of shadow estimations for optimizing the time of imagery collection with respect to the minimization of shadows. The optimization of imagery collection time is shown to be accomplished through the use of a global minimization search of the shadow estimation given a locations latitude and longitude. The rest of the paper is organized as follows. The following section briefly introduces object-based classification. In section III, the improvement of the shadow classification is demonstrated, including in the case that the exact sun's position is unknown for a given set of imagery. Section IV describes the optimization of imagery collection timing with respect to shadow minimization. Finally, the paper concludes with observations for improvement.

II. Object-Based Classification

While the synergistic use of LiDAR and spectra data is not new, it has commonly been used with pixel-based classification methods such as maximum likelihood classifications where the high dimensionality of the data greatly increased the complexity without significant benefit. In an object-based classifier, the training data includes spatial, variability and texture based information and the classifier operates on small homogeneous regions as opposed to individual pixels. Objects are formed of multiple homogeneous regions based on all their relations (including spectral and spatial) and classified. Because of the wide variety of different objects that could be formed on the homogeneous regions, a process tree (Fig. 1) is commonly used.

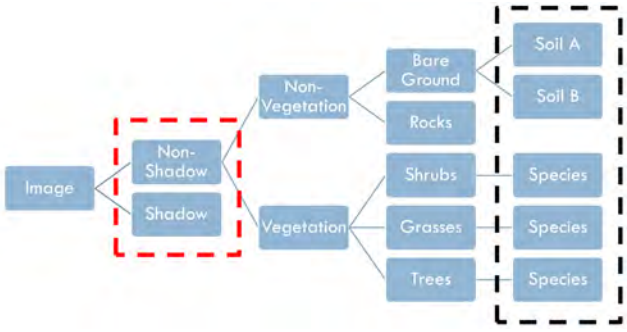

Figure 1. Object-Based Classification Tree

In this process, the image is sequentially classified, first by isolating shadows from non-shadows, followed by vegetation from non-vegetation and so on until the desired level of classification is achieved. This object-based classification with process tree has shown significant applicability for high resolution aerial imagery applications [4,17]. For the best performance at the desired classification (identified in dashed black), the classification must be as accurate as possible at the top layers of the process tree, in this case the estimation of shadow vs non-shadow objects (identified in dashed red).

III. Shadow Classification Improvement

Shadows negatively effect vegetation indices and should be ignored for the purposes of classification, thus it is important that they are removed before further classification occurs. However, objects that are shaded from the sun may still be illuminated from ambient surfaces, making it difficult to use RGB bands for identification. The NIR band of imagery provides the best source for segregating shadow from other features, however, it is also a good indicator of water (Fig. 2). To differentiate between water and shadow, a digital elevation model (DEM) can be used to predict where shadows would fall.

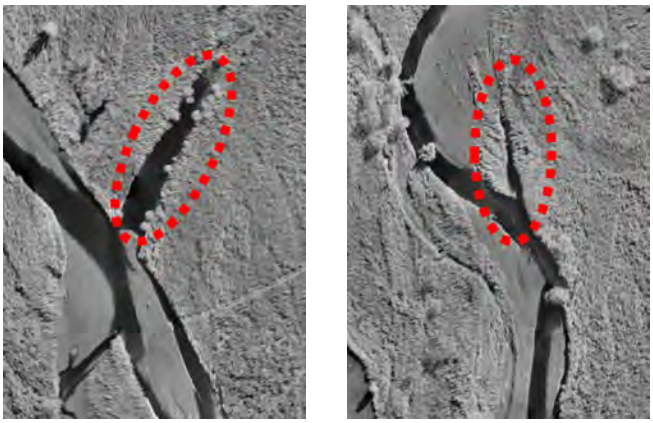

(a) NIR Imagery of Water (b) NIR Imagery of Shadow

Figure 2. NIR Imagery - ROI indicated with red dotted line

In this paper, DEMs are generated using Agisoft Photoscan using a Structure-from-Motion (SfM) algorithm. An example of a DEM and subsequent shadow estimation can be seen in Fig. 3. Utilizing a SfM algorithm, all that is required is a sufficient overlap of imagery and ground control points. This eliminates the need to carry extra equipment such as LiDAR. The accuracy of a DEM created in this method is not as accurate as LiDAR, but is sufficient and comparable to the accuracy of the georeference orthographic image [14].

With a DEM, a shadow estimate can be created. In this paper, the shadow was estimated using a hillshading algorithm within ArcGIS [19], but any shadow estimation algorithm could be used. The use of hillshade maps are commonly found in geographic information system (GIS) research. With the advent of LiDAR generated DEM, hillshade maps have been utilized for such applications as historical landslide detection [20] and solar radiance analysis studies [21,22]. Many hillshade algorithms implemented in commercially available software such as ArcGIS or the open-source SAGA-GIS [23] include options for ray-trace calculations for cast shadows. Algorithms for such calculations are also available through existing literature as well [24]. However, in all shadow estimating algorithms, the sun's position, the azimuth and elevation, must be known. While most electronics have internal clocks that can be used as a reference to calculate

(a) Digital Elevation Model (DEM)

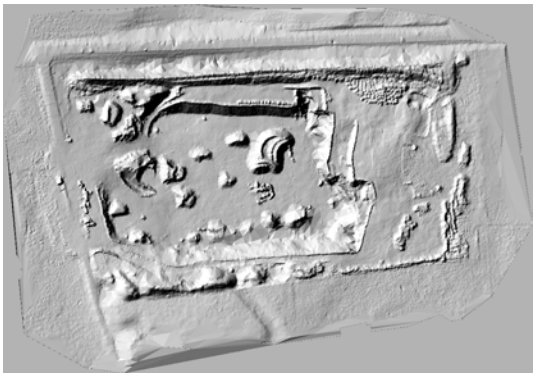

(b) Shadow Estimation using Hillshade

Figure 3. DEM and Shadow Estimation [18]

the sun's position given a location, time and date, it can be shown that the sun's position can also be calculated from the imagery alone by using a simple global search. Using the NIR band as a reference, the global search finds the sun's azimuth and elevation that corresponds to the highest correlation of estimate and NIR band response. This can be solved with any local min/max search function by formulate the problem into a search

$$\min_{\alpha,\phi} -NIR\,(x,y,i) \bigcap Shadow(x,y,i,\alpha,\phi) \text{ for } \forall x,y \in \mathcal{I} \tag{1}$$

where $x, y \in \mathcal{I}$ represent all pixels within image $\mathcal{I}$, i represents pixel intensity, α represents the sun's azimuth and ϕ is the sun's elevation angle. An image of the shadow estimate generated with a value forα and ϕ is used to compare to the reference NIR image. When comparing the generated shadow map with the NIR reference, shadows would be signified by a low response in NIR and the shadow estimate, whereas water would only have the low response in NIR. The sun's position, represented by α and ϕ, occurs at the corresponding values at which the estimated shadow map and NIR image have the highest correlation.

The global search was run with the NIR band image (Fig. 4). The orientation of the shadow estimation was run based on local orientation as opposed to true north orientation. Fig. 4 depicts the true North orientation of the image used, with

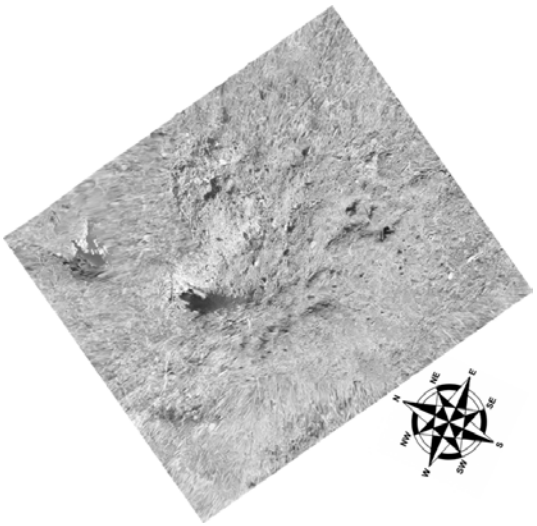

Figure 4. Reference NIR Image

North rotated by $65°$ counter clockwise and tilted by $10°$ due to imagery collection bias. The imagery was taken at $37.375774°$, $-120.57847°$, set at UTC-08:00. Local time of image collection was between 10:59 and 11:05 AM.

The results of the global search can be seen in Fig 5. In this paper, a brute force approach with coarse steps was applied to illustrate the existence of a global singular minimum. A more elegant search algorithm could be performed and would provide finer results.

The correlation between the reference image and the sun's azimuth and elevation angle can be seen in Fig. 6. The resulting surface plot shows a global minimum at an estimate of azimuth at $100°$ and an elevation at $40°$ relative to the imagery. Adjusted for imagery rotation, this corresponds with the published sun azimuth and elevation of $166°$ and $29°$, as given by the NOAA Solar Calculator [25].

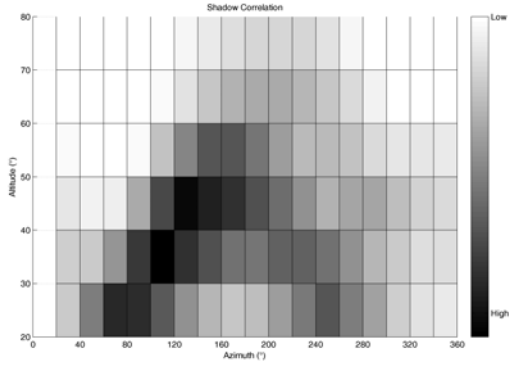

Figure 6. Correlation of Estimate as a function of sun's azimuth and elevation

Shown that a shadow estimate map is valid for predicting shadows enough to back calculate a sun's position, it follows that it is valid enough to be utilized for both the classification process. ENVI Ex with the Feature Extraction (FE) module [26] was utilized for the classification of the imagery. The RGB and NIR band imagery was set as the base imagery with the shadow estimation and DEM data added as ancillary data. The base imagery is segmented into small homogeneous regions and training data is used to connect the segments to form objects. In this classification, three regions were identified: shadow, vegetation and non-vegetation. The results of the shadow classification can be seen in Fig. 7. In Fig. 7a, no shadow estimation was added. The segmentation resulted in poor classification as it was unable to separate the finer shadows. In Fig. 7b, the segmentation performed significantly better.

IV. Optimal Time of Data Collection

In the previous section, the DEM and subsequent shadow estimation enabled improved classification performance. However, further improvements can be achieved through the optimal collection of imagery with respect to the minimization of shadowing effect. In applications such as rangeland management where the region of interest has significant heterogeneity in elevation, shadows can have significant negative effects on analysis. The validation of the previous sections implementation of a global search for estimating the sun's position given a shadow map compared to an NIR image is used to justify the value of using shadow estimation algorithms for generating shadow maps that are used in the optimization process.

Given a location's latitude and longitude, the NOAA Solar Calculator can plot the sun's azimuth and solar elevation for any given day [25]. The shadow estimation can be run over the set of azimuth and solar elevation angle for a given day and time. The optimization can be formed into a minimization function

$$\min_{t} Shadow(x, y, \alpha, \phi) \text{ for } \forall x, y \in \mathcal{I} \tag{2}$$

where estimated sun's α and ϕ can is calculated through the NOAA Solar calculator, and $x, y \in \mathcal{I}$ represents all pixels within image $\mathcal{I}$. The shadow estimation can be calculated through any means, though in this paper was calculated through a hillshading algorithm within ArcGIS [19]. The minimization function is designed to find the time t at which there is the least amount of shadowing on the image. In many cases, the minimization is achieved at solar noon, however in many topographically challenging locations, this may not be the case.

The result of the optimization run on the small hill (Fig. 4) can be seen in Fig. 8. As expected, as the sun reaches its solar noon (at t = 12.26 hr), the shadow intensity decreases. However, the optimal time for collecting imagery for the date of February 15, 2014 would be at 13:00hr or 34 minutes after solar noon. As a reference for time scale, the process for data collection of this imagery set took approximately 10 minutes including the takeoff and landing.

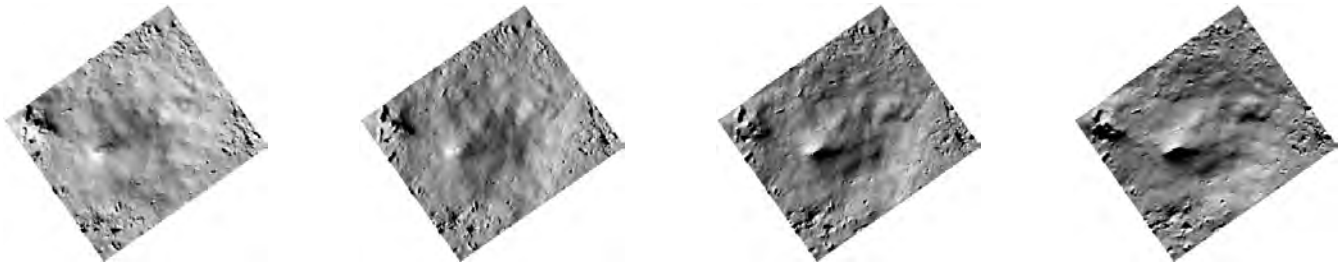

(a) Azimuth: 40 degrees (b) Azimuth: 80 degrees (c) Azimuth: 120 degrees (d) Azimuth: 160 degrees

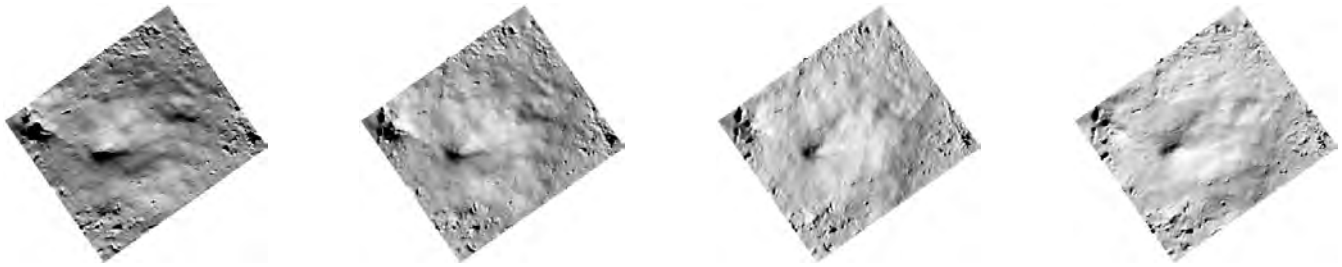

(e) Azimuth: 200 degrees (f) Azimuth: 240 degrees (g) Azimuth: 280 degrees (h) Azimuth: 320 degrees

Figure 5. Shadow Estimation at Elevation 40 degrees

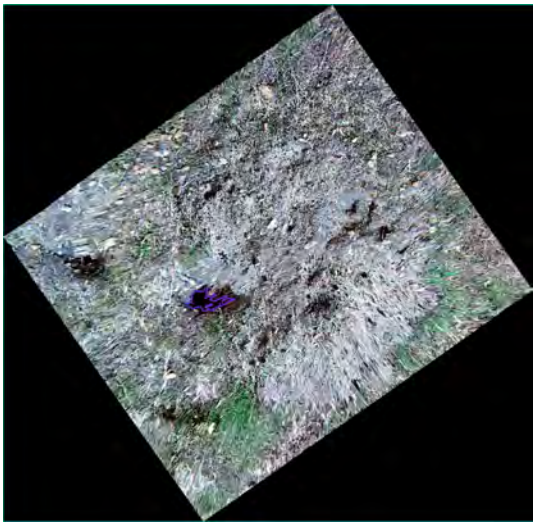

(a) Original Processing

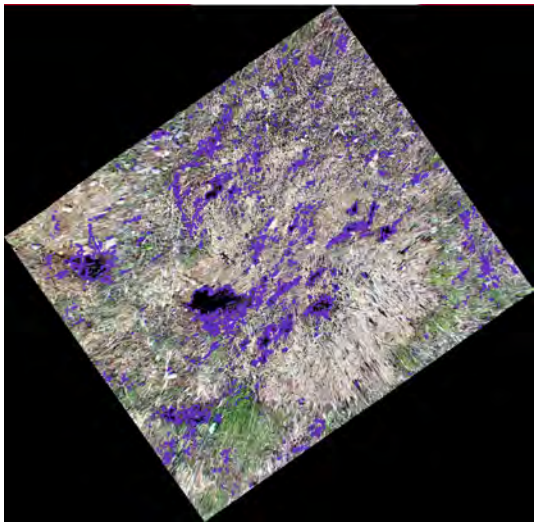

(b) With Shadow Estimator

Figure 7. Shadow Classification Results

V. Conclusion

The use of a DEM for shadow estimation can be beneficial for both improved shadow classification and for the optimization of the time of imagery collection. Shadow estimation is a simple adjustment to the classification process that shows significant potential benefit. In this paper, the results presented are of simple cases, but the concept remains valid. Further expansion should be taken on evaluating and testing different shadow estimation techniques. Hill shading is sufficient for sloping terrains, but is less accurate at higher slope angles and low elevation angles. One caveat, is that the addition of more information does not always improve classification performance. Increased complexity from higher dimensionality can lead to unintended consequences and over training, thus it is important that the addition of another dimension of data be significant. As shown in this paper, the addition of a shadow estimated built by a DEM adds enough valuable information to justify the extra dimensionality. The new data weights crowded and diverse heterogeneity vegetation and non-vegetation against a more general shadow profile enabling higher separability, while also providing a significant way to distinguish shadows from water features.

The optimization of the time of imagery collection is also enabled through the estimation of shadows generated from

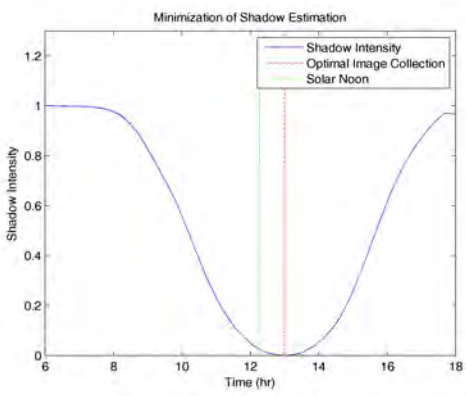

Figure 8. Minimization of shadow

a DEM. The optimization can be formed through a simple minimization function that could be further refined for better results. The most important aspect is that these improvements are accomplished without adding extra sensors or equipment to a UAS since it relies solely on the data already collected. As more and more remote sensing applications are developed, it is important that developers find ways to utilize the data already collected to extract as much information as possible given the limited payload capacity of a UAS.

REFERENCES

[1] P. J. Hardin and M. W. Jackson, "An Unmanned Aerial Vehicle for Rangeland Photography," *Rangeland Ecology & Management*, vol. 58, no. 4, pp. 439–442, 2005.

[2] R. P. Breckenridge, M. Dakins, S. Bunting, J. L. Harbour, and S. White, "Comparison of unmanned aerial vehicle platforms for assessing vegetation cover in Sagebrush Steppe ecosystems," *Rangeland Ecology & Management*, vol. 64, no. 5, pp. 521–532, 2011.

[3] J. J. Mitchell, N. F. Glenn, M. O. Anderson, R. C. Hruska, A. Halford, C. Baun, and N. Nydegger, "Unmanned Aerial Vehicle (UAV) Hyperspectral Remote Sensing for Dryland Vegetation Monitoring," in *Proc. of Whispers 4th Workshop on Hyperspectral Image and Signal Processing: Evolution in Remote Sensing*, 2012.

[4] A. S. Laliberte, J. E. Herrick, A. Rango, and C. Winters, "Acquisition, orthorectification, and object-based classification of unmanned aerial vehicle (UAV) imagery for rangeland monitoring," *Photogrammetric Engineering and Remote Sensing*, vol. 76, no. 6, pp. 661–672, 2010.

[5] Z. Song, Y. Chen, C. R. Sastry, and N. C. Tas, *Optimal Observation for Cyber-Physical Systems*. Springer, 2009.

[6] C. Tricaud and Y. Chen, *Optimal Mobile Sensing and Actuation Policies in Cyber-physical Systems*. Springer, 2012.

[7] H. Chao and Y. Chen, *Remote Sensing and Actuation Using Unmanned Vehicles*. John Wiley & Sons, 2012.

[8] E. Honkavaara, L. Markelin, T. Rosnell, and K. Nurminen, "Influence of solar elevation in radiometric and geometric performance of multispectral photogrammetry," *ISPRS Journal of Photogrammetry and Remote Sensing*, vol. 67, pp. 13–26, 2012.

[9] H. G. Jones and R. A. Vaughan, *Remote Sensing of Vegetation*. Oxford University Press, 2010.

[10] P. R. Wolf, B. A. Dewitt, and B. Wilkinson, *Elements of Photogrammetry with Applications in GIS*. McGraw-Hill, 4 ed., 2014.

[11] A. M. Jensen, T. Hardy, M. McKee, and Y. Q. Chen, "Using a multispectral autonomous unmanned aerial remote sensing platform (AggieAir) for riparian and wetlands applications," in *Proc. of 2011 IEEE International Geoscience and Remote Sensing Symposium (IGARSS)*, pp. 3413–3416, 2011.

[12] B. Koetz, F. Morsdorf, S. Van der Linden, T. Curt, and B. Allgöwer, "Multi-source land cover classification for forest fire management based on imaging spectrometry and LiDAR data," *Forest Ecology and Management*, vol. 256, no. 3, pp. 263–271, 2008.

[13] G. Rock, J. Ries, and T. Udelhoven, "Sensitivity Analysis of UAV-Photogrammetry for Creating Digital Elevation Models (DEM)," in *Proc. of Conference on Unmanned Aerial Vehicle in Geomatics*, 2011.

[14] L. Javernick, J. Brasington, and B. Caruso, "Modelling the topography of shallow braided rivers using Structure-from-Motion photogrammetry," *Geomorphology*, vol. 213, pp. 166–182, 2014.

[15] K. Whitehead, B. Moorman, and C. Hugenholtz, "Low-cost, on-demand aerial photogrammetry for glaciological measurement," *Cryosphere Discussions*, vol. 7, no. 3, 2013.

[16] C.-T. Wu, C.-Y. Hsiao, and P.-S. Hsieh, "Using UAV and VBS-RTK for Rapid Reconstruction of Environmental 3D Elevation Data of the Typhoon Morakot Disaster Area and Disaster Scale Assessment," *Journal of Chinese Soil and Water Conservation*, vol. 44, no. 1, pp. 23–33, 2013.

[17] A. S. Laliberte, M. A. Goforth, C. M. Steele, and A. Rango, "Multispectral remote sensing from unmanned aircraft: image processing workflows and applications for rangeland environments," *Remote Sensing*, vol. 3, no. 11, pp. 2529–2551, 2011.

[18] Trimble UAS, "Trimble UAS." [ONLINE] http://uas.trimble.com/, 2014.

[19] ESRI, "ArcGIS - Mapping and Spatial Analysis." [ONLINE] http://www.esri.com/software/arcgis, 2014.

[20] M. Van Den Eeckhaut, J. Poesen, G. Verstraeten, V. Vanacker, J. Moeyersons, J. Nyssen, and L. Van Beek, "The effectiveness of hillshade maps and expert knowledge in mapping old deep-seated landslides," *Geomorphology*, vol. 67, no. 3, pp. 351–363, 2005.

[21] L. Kumar, A. K. Skidmore, and E. Knowles, "Modelling topographic variation in solar radiation in a GIS environment," *International Journal of Geographical Information Science*, vol. 11, no. 5, pp. 475–497, 1997.

[22] K. Zakšek, T. Podobnikar, and K. Oštir, "Solar radiation modelling," *Computers & Geosciences*, vol. 31, no. 2, pp. 233–240, 2005.

[23] SAGA User Group Association, "SAGA - System for Automated Geoscientific Analyses." [ONLINE] http://www.saga-gis.org/, 2014.

[24] P. T. Giles, "Remote sensing and cast shadows in mountainous terrain," *Photogrammetric Engineering and Remote Sensing*, vol. 67, no. 7, pp. 833–840, 2001.

[25] National Oceanic & Atmospheric Administration, "NOAA Solar Calculator." [ONLINE] http://www.esrl.noaa.gov/gmd/grad/solcalc/, 2013.

[26] Exelis Visual Information Solutions, "ENVI Software - Image Analysis Software." [ONLINE] https://www.exelisvis.com/ProductsServices/ENVI/ENVI.aspx, 2014.